

We are IntechOpen, the world's leading publisher of Open Access books Built by scientists, for scientists

6,900

Open access books available

186,000

International authors and editors

200M

Downloads

Our authors are among the

154

Countries delivered to

TOP 1%

most cited scientists

12.2%

Contributors from top 500 universities



WEB OF SCIENCE™

Selection of our books indexed in the Book Citation Index
in Web of Science™ Core Collection (BKCI)

Interested in publishing with us?
Contact book.department@intechopen.com

Numbers displayed above are based on latest data collected.
For more information visit www.intechopen.com



An Analytical Solution for Inhomogeneous Strain Fields Within Wurtzite GaN Cylinders Under Compression Test

X. X. Wei

*State Key Laboratory of Explosion Science and Technology,
Beijing Institute of Technology,
China*

1. Introduction

Compression test on solid circular cylinders of finite length is a popular method in obtaining the compressive strength, the elastic moduli and the electronic properties of semiconductors (Goroff & Kleinman, 1963; Pollak & Cardona, 1968). It was found that, by generating a strain field, the external stress may significantly change the electronic energy structures and the optoelectronic behavior of semiconductors (Suzuki & Hensel, 1974; Mathieu et al, 1979; Bir & Pickus, 1974; Singh, 1992; Pollak, 1990). Several methods have been used to investigate the effect of stress and strain on band structures (Jiang & Singh, 1997; Hasegawa, 1963). For example, the multiband effective-mass theory was employed to study the electronic and optical-absorption properties of uniaxially stressed quantum wells, the envelope-function approximation was used to describe the electronic structure of superlattices and quantum wells under arbitrary uniaxial stress, the effect of uniaxial and hydrostatic strain on the optical constants and the electronic structure of Copper was investigated, the strain dependence of effective masses in tetrahedral semiconductor under uniaxial stress was also studied. In all of these studies, the homogeneous strain distributions induced by an external uniform stress were considered. Pollak (1990) made good review on the effect of homogeneous strain on band structures and electronic properties of semiconductors.

However, friction effect on the end surfaces is ignored in all of these studies. It has long been recognized that friction inevitably exists between two end surfaces of cylinders and the loading platens under compression test. The strain and stress distributions within cylinder are very sensitive to the external load acting on the surface of cylinders (Wei et al, 1999). Although numerous efforts have been made to reduce the friction between the semiconductor cylinder and the loading platens, end friction inevitably exists. Techniques developed to reduce end friction include the insertion of Telfon sheet, lubrication, iron brush contact, and the use of a loading platen of the same Poisson's ratio as the cylinder. Nevertheless, the stress distributions within cylinders under compression are normally non-uniform, and inhomogeneous strain fields are thus induced within semiconductor cylinders. Although the analytical solution for finite cylinders under arbitrary external load was obtained (Chau & Wei, 1999), the solution is for isotropic materials with force boundary condition only. Experimental results show that wurtzite GaN is a kind of transversely

isotropic crystal. There is no analysis for the inhomogeneous strain distributions within wurtzite GaN cylinders due to end friction under compression tests.

Therefore, in the present work, the inhomogeneous strain distribution within a finite and transversely isotropic cylinder of wurtzite GaN subject to compression with non-zero end friction is studied. The friction between the end surfaces and two loading platens will be modeled as non-slip as well as partially slip. Unlike the force boundary condition for finite cylinders (Wei & Chau, 1999; Chau & Wei, 1999), displacement boundary condition will have to be involved in the present problem. The Lekhnitskii's stress function is employed in order to uncouple the equations of equilibrium for transversely isotropic solids. The Fourier and Fourier-Bessel expansion technique will be used in order to satisfy all of the boundary conditions exactly. In addition, Based on the theory of Luttinger-Kohn and Bir-Pikus (Bir & Pikus, 1974), the valence-band structure of the strained wurtzite GaN is described by a Hamiltonian in the envelope-function space, and the spin-orbit interaction is also considered, numerical discussion will focus on the effects of strain and end friction on the band structure of wurtzite GaN.

2. Governing equations for wurtzite GaN solid

Experimental results show that wurtzite GaN is a kind of transversely isotropic solids (Wright, 1997). Let's consider a homogeneous wurtzite GaN cylinder of radius R and half-length h with the two end surfaces parallel to a plane of isotropy.

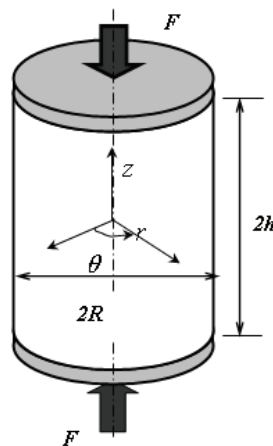


Fig. 1. A sketch of a finite cylinder under compression test

For the cylindrical coordinate system (r, θ, z) shown in Fig.1, the generalized Hooke's law for transversely isotropic solids can be written as (Wei, 2008)

$$\begin{aligned} \varepsilon_{rr} &= a_{11}\sigma_{rr} + a_{12}\sigma_{\theta\theta} + a_{13}\sigma_{zz}, & \varepsilon_{\theta\theta} &= a_{12}\sigma_{rr} + a_{11}\sigma_{\theta\theta} + a_{13}\sigma_{zz} \\ \varepsilon_{zz} &= a_{13}\sigma_{rr} + a_{13}\sigma_{\theta\theta} + a_{33}\sigma_{zz}, & \gamma_{\theta z} &= a_{44}\sigma_{\theta z}, \gamma_{rz} = a_{44}\sigma_{rz}, \gamma_{r\theta} = a_{66}\sigma_{r\theta} \end{aligned} \quad (1)$$

where

$$\begin{aligned} a_{11} &= \frac{1}{E_T}, & a_{12} &= -\frac{\nu_T}{E_T}, & a_{13} &= -\frac{\nu_L}{E_L}, & a_{33} &= \frac{1}{E_L}, \\ a_{44} &= \frac{1}{G_L}, & a_{66} &= 2(a_{11} - a_{12}) = \frac{2(1 + \nu_T)}{E_T} = \frac{1}{G_T} \end{aligned} \quad (2)$$

The stress tensor is denoted by σ , and the normal and shear strains by ε and γ respectively. Physically, E_T and E_L are the Young's moduli governing axial deformations in the planes of isotropy (i.e. any plane parallel to two end surfaces) and along direction perpendicular to it (i.e. parallel to the z -axis) respectively. The Poisson's ratios ν_T and ν_L characterize transverse reductions in the plane of isotropy under tension in the same plane and under tension along the z -axis respectively. The shear moduli for the plane of isotropy and for planes parallel to the z -axis are denoted by G_T and G_L , respectively. For present axisymmetric problem, strains and displacements are related by

$$\varepsilon_{rr} = \frac{\partial u}{\partial r}, \varepsilon_{\theta\theta} = \frac{u}{r}, \varepsilon_{zz} = \frac{\partial w}{\partial z}, \varepsilon_{rz} = \frac{1}{2} \left(\frac{\partial u}{\partial z} + \frac{\partial w}{\partial r} \right) \quad (3)$$

where u and w are the displacements in the r - and z -directions, respectively. In the absence of body force, the equations of equilibrium are

$$\frac{\partial \sigma_{rr}}{\partial r} + \frac{\partial \sigma_{rz}}{\partial z} + \frac{\sigma_{rr} - \sigma_{\theta\theta}}{r} = 0 \quad (4)$$

$$\frac{\partial \sigma_{zz}}{\partial z} + \frac{\partial \sigma_{rz}}{\partial r} + \frac{\sigma_{rz}}{r} = 0 \quad (5)$$

3. Uniform strain in cylinders under compression without end friction

When a solid cylinder of wurtzite GaN is confined by a uniform pressure p_0 on the curved surface and is compressed between two rigid smooth loading platens on the end surfaces without end friction. The stresses within the solid cylinder are uniform and can be expressed as

$$\sigma_{zz} = q_0, \quad \sigma_{rr} = \sigma_{\theta\theta} = p_0, \quad \sigma_{rz} = \sigma_{r\theta} = \sigma_{\theta z} = 0 \quad (6)$$

where $q_0 = F / \pi R^2$ with F being the total load acting on the end surfaces as shown in Fig. 1. By adopting the usual sign convention of continuum mechanics, tension is positive, and compression is negative.

The strains within the cylinder can be obtained by substituting (6) into (1) as:

$$\varepsilon_{zz} = \left(-\frac{2\nu_L p_0}{q_0} + 1 \right) \frac{q_0}{E_L}, \quad \varepsilon_{rr} = \varepsilon_{\theta\theta} = \left[(1 - \nu_T) \frac{E_L p_0}{E_T q_0} - \nu_L \right] \frac{q_0}{E_L}, \quad \gamma_{rz} = \gamma_{r\theta} = \gamma_{z\theta} = 0 \quad (7)$$

It is obvious that inhomogeneous strain field is induced within cylinder under compression if the end friction is ignored.

4. Boundary conditions for compression with end friction

Friction, however, always inevitably exists between the loading platens and the two end surfaces in usual compression tests. The end surfaces are thus somewhat constrained from free expansion of the Poisson effect. The boundary conditions for a solid cylinder under compression test with end friction and a confine pressure p_0 can be written as

$$\sigma_{rr} = p_0, \quad \text{on } r = R \quad (8)$$

$$\sigma_{rz} = 0, \quad \text{on } r = R \quad (9)$$

$$u = \beta u_0 r / R, \quad \text{on } z = \pm h, \quad (10)$$

$$\frac{\partial w}{\partial r} = 0, \quad \text{on } z = \pm h, \quad (11)$$

$$\int_0^R 2\pi r \sigma_{zz} dr = F, \quad \text{on } z = \pm h \quad (12)$$

where F is the total load acting on the loading platens. Physically, these boundary conditions imply that the cylinder is subjected to an axial compression of magnitude F with confining stress of p_0 and with no end rotation. Boundary condition (10) implies a uniform radial strain on the two end surfaces, and (11) ensures to loading platens to remain horizontal at all time, The factor β represents the degree of constraint on the radial displacement on the end surfaces. If friction is negligible, the end surface is free to expand and we have $\beta = 1$; if the radial displacement on the end surfaces is completely constrained, no slip occurs between the cylinder and loading platens and we have $\beta = 0$; in usual compression test, we have $0 \leq \beta \leq 1$, depending on the contact condition of the loading platens.

5. Stress function for transversely isotropic solids

As suggested by Lekhnitskii (1963), a single stress function ϕ can be introduced for transversely isotropic solids as

$$\sigma_{rr} = -\frac{\partial}{\partial z} \left(\frac{\partial^2 \phi}{\partial r^2} + \frac{b}{r} \frac{\partial \phi}{\partial r} + e \frac{\partial^2 \phi}{\partial z^2} \right) \quad (13)$$

$$\sigma_{\theta\theta} = -\frac{\partial}{\partial z} \left(b \frac{\partial^2 \phi}{\partial r^2} + \frac{1}{r} \frac{\partial \phi}{\partial r} + e \frac{\partial^2 \phi}{\partial z^2} \right) \quad (14)$$

$$\sigma_{zz} = \frac{\partial}{\partial z} \left(c \frac{\partial^2 \phi}{\partial r^2} + \frac{c}{r} \frac{\partial \phi}{\partial r} + d \frac{\partial^2 \phi}{\partial z^2} \right) \quad (15)$$

$$\sigma_{rz} = \frac{\partial}{\partial r} \left(\frac{\partial^2 \phi}{\partial r^2} + \frac{1}{r} \frac{\partial \phi}{\partial r} + e \frac{\partial^2 \phi}{\partial z^2} \right) \quad (16)$$

$$u = -(1-b)(a_{11} - a_{12}) \frac{\partial^2 \phi}{\partial r \partial z} \quad (17)$$

$$w = a_{44} \left(\frac{\partial^2 \phi}{\partial r^2} + \frac{1}{r} \frac{\partial \phi}{\partial r} \right) + (a_{33}d - 2a_{13}e) \frac{\partial^2 \phi}{\partial z^2} \quad (18)$$

where

$$\begin{aligned}
 b &= \frac{a_{13}(a_{13} + a_{44}) - a_{12}a_{33}}{a_{11}a_{33} - a_{13}^2}, & c &= \frac{a_{13}(a_{11} - a_{12}) + a_{11}a_{44}}{a_{11}a_{33} - a_{13}^2} \\
 d &= \frac{a_{11}^2 - a_{12}^2}{a_{11}a_{33} - a_{13}^2}, & e &= \frac{a_{13}(a_{11} - a_{12})}{a_{11}a_{33} - a_{13}^2}
 \end{aligned}
 \tag{19}$$

To ensure force equilibrium, the stress function ϕ should satisfy the following partial differential equation

$$\left(\frac{\partial^2}{\partial r^2} + \frac{1}{r} \frac{\partial}{\partial r}\right)\left(\frac{\partial^2 \phi}{\partial r^2} + \frac{1}{r} \frac{\partial \phi}{\partial r} + e \frac{\partial^2 \phi}{\partial z^2}\right) + \frac{\partial^2}{\partial z^2}\left(c \frac{\partial^2 \phi}{\partial r^2} + \frac{c}{r} \frac{\partial \phi}{\partial r} + d \frac{\partial^2 \phi}{\partial z^2}\right) = 0
 \tag{20}$$

6. Series expressions for the stress function

We seek for the following series solution forms for (20) as

$$\phi = \sum_{n=1}^{\infty} A'_n I_0(p \zeta_n \rho) \sin(n\pi\eta) \quad \text{and} \quad \phi = \sum_{s=1}^{\infty} C'_s \sinh(q \gamma_s \eta) J_0(\lambda_s \rho)
 \tag{21}$$

where $\rho = r / R$, $\eta = z / h$, λ_s is the s -th root of $J_1(\lambda_s) = 0$; $\gamma_s = \lambda_s \kappa$ and $\zeta_n = n\pi / \kappa$; κ is a geometric ratio defined as $\kappa = h / R$; p and q are constants to be determined. A'_n and C'_s are constants. $J_0(x)$ and $J_1(x)$ are the Bessel functions of the first kind of zero and first order respectively, and $I_0(x)$ is the modified Bessel function of the first kind of zero order.

Substitution of (21) into (20) yields

$$q_{1,2} = \left[\frac{(c + e) \pm \sqrt{(c + e)^2 - 4}}{2} \right]^{1/2}, \quad q_{3,4} = -q_{1,2}, \quad \text{and} \quad p_{1,2} = q_{1,2}, \quad p_{3,4} = -p_{1,2}
 \tag{22}$$

By noting the fact that $I_0(-x) = I_0(x)$ and $\sinh(-x) = -\sinh(x)$, it is clear from (21) that the solutions corresponding to $p_{3,4}$ and $q_{3,4}$ can be combined with those for $p_{1,2}$ and $q_{1,2}$. It has been found that $q_{1,2}$ are complex for wurtzite GaN solid. That is, $q_{1,2}$ can be expressed in form of $q_{1,2} = q_R \pm q_I i$, so we can rewrite the expression for stress function ϕ as

$$\begin{aligned}
 \phi &= -R^3 q_0 \left\{ A_0 \frac{\kappa^3 \eta^3}{6} + C_0 \frac{\kappa \eta \rho^2}{2} + \sum_{n=1}^{\infty} \frac{\sin(n\pi\eta)}{\zeta_n^3} \{ A_n \operatorname{Re}[I_0(p_1 \zeta_n \rho)] + B_n \operatorname{Im}[I_0(p_1 \zeta_n \rho)] \} \right. \\
 &\quad \left. + \sum_{s=1}^{\infty} \frac{J_0(\lambda_s \rho)}{\lambda_s^3} [C_s \sinh(q_R \gamma_s \eta) \cos(q_I \gamma_s \eta) + D_s \cosh(q_R \gamma_s \eta) \sin(q_I \gamma_s \eta)] \right\}
 \end{aligned}
 \tag{23}$$

where q_0 is the mean normal stress on the end surfaces defined as $q_0 = P / \pi R^2$, and A_0, C_0, A_n, B_n, C_s , and D_s are real unknown constants to be determined. Note that additional terms corresponding to A_0 and C_0 have been added and they will lead to uniform normal stresses and strains for cylinders.

Before we consider the boundary conditions (8-12), stresses and displacements will first be expressed in terms of the unknown constants in the next section.

7. Expressions for stress and displacement components

Substitution of (23) into (13-18) yields the following expressions for the stress and displacement as

$$\begin{aligned} \sigma_{rr} / q_0 = & A_0 e + (a+b)C_0 + \sum_{n=1}^{\infty} \cos(n\pi\eta) \{A_n \operatorname{Re}[\Pi_1(p_1, \rho)] + B_n \operatorname{Im}[\Pi_1(p_1, \rho)]\} \\ & + \sum_{s=1}^{\infty} \{ [C_s \Lambda_1(q_R, q_I, \rho) + D_s \Lambda_2(q_R, q_I, \rho)] \cosh(q_R \gamma_s \eta) \cos(q_I \gamma_s \eta) \\ & + [-C_s \Lambda_2(q_R, q_I, \rho) + D_s \Lambda_1(q_R, q_I, \rho)] \sinh(q_R \gamma_s \eta) \sin(q_I \gamma_s \eta) \} \end{aligned} \quad (24)$$

$$\begin{aligned} \sigma_{rz} / q_0 = & \sum_{n=1}^{\infty} \sin(n\pi\eta) \{A_n \operatorname{Re}[\Pi_2(p_1, \rho)] + B_n \operatorname{Im}[\Pi_2(p_1, \rho)]\} \\ & + \sum_{s=1}^{\infty} J_1(\lambda_s \rho) \{ [C_s (e^{q_R^2} - q_I^2) - 1] + 2D_s e q_R q_I \} \sinh(q_R \gamma_s \eta) \cos(q_I \gamma_s \eta) \\ & + [-2C_s e q_R q_I + D_s (e^{q_R^2} - q_I^2) - 1] \cosh(q_R \gamma_s \eta) \sin(q_I \gamma_s \eta) \} \end{aligned} \quad (25)$$

$$\begin{aligned} \frac{u}{q_0 R} = & (1-b)(a_{11} - a_{12}) \{ C_0 \rho + \sum_{n=1}^{\infty} \frac{\cos(n\pi\eta)}{\zeta_n} \{ A_n \operatorname{Re}[p_1 I_1(p_1 \zeta_n \rho)] + B_n \operatorname{Im}[p_1 I_1(p_1 \zeta_n \rho)] \} \\ & - \sum_{s=1}^{\infty} \frac{J_1(\lambda_s \rho)}{\lambda_s} [(C_s q_R + D_s q_I) \cosh(q_R \gamma_s \eta) \cos(q_I \gamma_s \eta) + (-C_s q_I + D_s q_R) \sinh(q_R \gamma_s \eta) \sin(q_I \gamma_s \eta)] \} \end{aligned} \quad (26)$$

$$\begin{aligned} \frac{w}{q_0 R} = & -[2a_{44}C_0 + A_0(a_{33} - 2a_{13}e)]\kappa\eta + \sum_{n=1}^{\infty} \frac{\sin(n\pi\eta)}{\zeta_n} \{ A_n \operatorname{Re}[\Pi_3(p_1, \rho)] + B_n \operatorname{Im}[\Pi_3(p_1, \rho)] \\ & + \sum_{s=1}^{\infty} \frac{J_0(\lambda_s \rho)}{\lambda_s} \{ [C_s (a_{44} - (a_{33} - 2a_{13}e)(q_R^2 - q_I^2)) - 2D_s q_R q_I (a_{33} - 2a_{13}e)] \sinh(q_R \gamma_s \eta) \cos(q_I \gamma_s \eta) \\ & + [2C_s q_R q_I (a_{33} - 2a_{13}e) + D_s (a_{44} - (a_{33} - 2a_{13}e)(q_R^2 - q_I^2))] \cosh(q_R \gamma_s \eta) \sin(q_I \gamma_s \eta) \} \end{aligned} \quad (27)$$

where

$$\Pi_1(x, \rho) = (ax^2 - e)I_0(x\zeta_n\rho) + (b-a)x \frac{I_1(x\zeta_n\rho)}{\zeta_n\rho} \quad (28)$$

$$\Pi_2(x, \rho) = (ex - x^3)I_1(x\zeta_n\rho) \quad (29)$$

$$\Pi_3(x, \rho) = [-a_{44}x^2 + (a_{33} - 2a_{13}e)]I_0(x\zeta_n\rho) \quad (30)$$

$$\Gamma(\rho) = -aJ_0(\lambda_s\rho) + (a-b) \frac{J_1(\lambda_s\rho)}{\lambda_s\rho} \quad (31)$$

$$\Lambda_1(x, y, \rho) = x\Gamma(\rho) + e(x^3 - 3xy^2)J_0(\lambda_s\rho) \quad (32)$$

$$\Lambda_2(x, y, \rho) = y\Gamma(\rho) - e(y^3 - 3x^2y)J_0(\lambda_s\rho) \quad (33)$$

with $a=1$. The expression for $\sigma_{\theta\theta}$ can be obtained from (24) by replacing “ a ” and “ b ” by “ b ” and “ 1 ” respectively. While the expressions for σ_{zz} can be obtained from (24) by replacing both “ a ” and “ b ” by “ $-c$ ”, and “ e ” by “ $-d$ ” respectively. The next step is to use the boundary conditions (8-12) to determine the unknown coefficients.

8. Determination of unknown coefficients

The boundary condition $\sigma_{rz} = 0$ on the curved surface $\rho = 1$ (or $r = R$) leads to

$$A_n = E_n \operatorname{Im}[\Pi_2(p_1, 1)], \quad B_n = -E_n \operatorname{Re}[\Pi_2(p_1, 1)] \quad (34)$$

where E_n is a constant introduced to simplify the later presentation and it will be fixed later such that the subsequent formulas can be expressed in a more efficient manner.

The boundary condition $\partial w / \partial r = 0$ on the two end surfaces $\eta = \pm 1$ (i. e. $z = \pm h$) leads to

$$C_s = F_s \psi_1(q_R, q_I) \quad , \quad D_s = -F_s \psi_2(q_R, q_I) \quad (35)$$

where F_s is another constant introduced to simplify the subsequent presentation , and

$$\begin{aligned} \psi_1(q_R, q_I) = & -2q_R q_I (a_{33} - 2a_{13}e) \sinh q_R \gamma_s \cos q_I \gamma_s \\ & + [a_{44} - (a_{33} - 2a_{13}e)(q_R^2 - q_I^2)] \cosh q_R \gamma_s \sin q_I \gamma_s \end{aligned} \quad (36)$$

$$\begin{aligned} \psi_2(q_R, q_I) = & 2q_R q_I (a_{33} - 2a_{13}e) \cosh q_R \gamma_s \sin q_I \gamma_s \\ & + [a_{44} - (a_{33} - 2a_{13}e)(q_R^2 - q_I^2)] \sinh q_R \gamma_s \cos q_I \gamma_s \end{aligned} \quad (37)$$

The radial stress σ_{rr} on the curved surface $\rho = 1$ (i. e. $r = R$) can be obtained by setting $\rho = 1$ in (24) as

$$\begin{aligned} \sigma_{rr} / q_0 = & A_0 e + (a + b)C_0 + \sum_{n=1}^{\infty} \cos(n\pi\eta) \{A_n \operatorname{Re}[\Pi_1(p_1, 1)] + B_n \operatorname{Im}[\Pi_1(p_1, 1)]\} \\ & + \sum_{s=1}^{\infty} \{ [C_s \Lambda_1(q_R, q_I, 1) + D_s \Lambda_2(q_R, q_I, 1)] \cosh(q_R \gamma_s \eta) \cos(q_I \gamma_s \eta) \\ & + [-C_s \Lambda_2(q_R, q_I, 1) + D_s \Lambda_1(q_R, q_I, 1)] \sinh(q_R \gamma_s \eta) \sin(q_I \gamma_s \eta) \} \end{aligned} \quad (38)$$

By applying a Fourier expansion for the hyperbolic cosine in (38) and then expressing the result in terms of the constants E_n and F_s , we have

$$\sigma_{rr} / q_0 = A_0 e + (b + 1)C_0 + \sum_{s=1}^{\infty} F_s Q_{s0} / 2 + \sum_{n=1}^{\infty} [E_n \Delta_n + \sum_{s=1}^{\infty} F_s Q_{sn}] \cos(n\pi\eta) \quad (39)$$

where

$$\Delta_n = \text{Im}[\Pi_2(p_1, 1)]\text{Re}[\Pi_1(p_1, 1)] - \text{Re}[\Pi_2(p_1, 1)]\text{Im}[\Pi_1(p_1, 1)] \quad (40)$$

$$Q_{sn} = J_0(\lambda_s) \{ [T_1 \sinh q_R \gamma_s \cos q_I \gamma_s + T_2 \cosh q_R \gamma_s \sin q_I \gamma_s] L_{sn} + [T_3 \sinh q_R \gamma_s \cos q_I \gamma_s + T_1 \cosh q_R \gamma_s \sin q_I \gamma_s] G_{sn} \} \quad (41)$$

$$G_{sn} = 2(-1)^n \times \frac{[\gamma_s^2 q_R^2 + q_I^2 \gamma_s^2 + n^2 \pi^2] q_R \gamma_s \cosh q_R \gamma_s \sin q_I \gamma_s - [\gamma_s^2 q_R^2 + q_I^2 \gamma_s^2 - n^2 \pi^2] q_I \gamma_s \sinh q_R \gamma_s \cos q_I \gamma_s}{[\gamma_s^2 q_R^2 + (q_I \gamma_s - n\pi)^2][\gamma_s^2 q_R^2 + (q_I \gamma_s + n\pi)^2]} \quad (42)$$

$$T_1 = q_I \{ [a_{44} - (a_{33}d - 2a_{13}e)(q_R^2 - q_I^2)] [e(q_I^2 - 3q_R^2) + 1] - 2(a_{33}d - 2a_{13}e)q_R^2 [e(q_R^2 - 3q_I^2) - 1] \} \quad (43)$$

$$T_2 = q_R \{ [a_{44} - (a_{33}d - 2a_{13}e)(q_R^2 - q_I^2)] [e(q_R^2 - 3q_I^2) - 1] + 2(a_{33}d - 2a_{13}e)q_I^2 [e(q_I^2 - 3q_R^2) + 1] \} \quad (44)$$

$$T_3 = -q_R \{ [a_{44} - (a_{33}d - 2a_{13}e)(q_R^2 - q_I^2)] [e(q_R^2 - 3q_I^2) - 1] + 2(a_{33}d - 2a_{13}e)q_I^2 [e(q_R^2 - 3q_I^2) + 1] \} \quad (45)$$

The boundary condition $\sigma_{rr} = 0$ on $\rho = 1$ can now be applied and the following relations between A_0 and C_0 and between E_n and F_s are obtained as

$$A_0 e + (b+1)C_0 + \sum F_s Q_{s0} / 2 = 0 \quad (46)$$

$$E_n \Delta_n + \sum_{s=1}^{\infty} F_s Q_{sn} = 0 \quad (47)$$

Substitution of (34) and (35) into (26) and set $\eta = \pm 1$ yield the following expression for the radial displacement on the two end surfaces (i.e. $z = \pm h$)

$$\frac{u}{q_0 R} = (1-b)(a_{11} - a_{12}) \{ C_0 \rho + \sum_{n=1}^{\infty} \frac{(-1)^n E_n}{\zeta_n} [\text{Im}[\Pi_2(p_1, 1)]\text{Re}[p_1 I_1(p_1 \zeta_n \rho)] - \text{Re}[\Pi_2(p_1, 1)]\text{Im}[p_1 I_1(p_1 \zeta_n \rho)]] + \sum_{s=1}^{\infty} \frac{J_1(\lambda_s \rho) F_s}{\lambda_s} \Omega_s \} \quad (48)$$

where

$$\Omega_s = -\{ [\psi_1(q_R, q_I)q_R - \psi_2(q_R, q_I)q_I] \cosh q_R \gamma_s \cos q_I \gamma_s - [\psi_1(q_R, q_I)q_I + \psi_2(q_R, q_I)q_R] \sinh q_R \gamma_s \sin q_I \gamma_s \} \quad (49)$$

To apply the end boundary condition (11), we first expand (48) into a Fourier-Bessel series as

$$\frac{u}{q_0 R} = (1-b)(a_{11} - a_{12}) \sum_{s=1}^{\infty} \frac{J_1(\lambda_s \rho)}{\lambda_s} \left[-\frac{2C_0}{J_0(\lambda_s)} + F_s \Omega_s + \sum_{n=1}^{\infty} E_n R_{sn} \right] \quad (50)$$

where

$$R_{sn} = \frac{(-1)^n}{\zeta_n} \{ \text{Im}[\Pi_2(p_1, 1)] \text{Re}[H_{sn}(p_1)] - \text{Re}[\Pi_2(p_1, 1)] \text{Im}[H_{sn}(p_1)] \} \quad (51)$$

$$H_{sn}(x) = \frac{-2x\lambda_s^2 I_1(x\zeta_n)}{[\lambda_s^2 + \zeta_n^2 x^2] J_0(\lambda_s)} \quad (52)$$

To match the boundary condition (11) with the radial displacement given in (50), (11) is also expanded into a Fourier-Bessel series as

$$u(\rho) = \beta u_0 \sum_{s=1}^{\infty} a_s J_1(\lambda_s \rho) \quad \text{for } (0 \leq \rho \leq 1) \quad (53)$$

where

$$a_s = \frac{-2}{\lambda_s J_0(\lambda_s)} \quad (54)$$

Finally, by comparing the coefficients of (50) and (53), we have

$$-\frac{2C_0}{J_0(\lambda_s)} + F_s \Omega_s + \sum_{n=1}^{\infty} E_n R_{sn} = \frac{-\nu u_0}{(1-b)(a_{11} - a_{12})} \frac{\beta \lambda_s a_s}{E} \quad (55)$$

As remarked earlier, the expressions for σ_{zz} can be obtained by replacing both "a" and "b" by "-c", and "e" by "-d" in (24) as

$$\begin{aligned} \sigma_{zz} / q_0 = & -A_0 - 2cC_0 + \sum_{n=1}^{\infty} \cos(n\pi\eta) \{ A_n \text{Re}[\Pi_1(p_1, \rho)] + B_n \text{Im}[\Pi_1(p_1, \rho)] \} \\ & + \sum_{s=1}^{\infty} \{ [C_s \Lambda_1(q_R, q_I, \rho) + D_s \Lambda_2(q_R, q_I, \rho)] \cosh(q_R \gamma_s \eta) \cos(q_I \gamma_s \eta) \\ & + [-C_s \Lambda_2(q_R, q_I, \rho) + D_s \Lambda_1(q_R, q_I, \rho)] \sinh(q_R \gamma_s \eta) \sin(q_I \gamma_s \eta) \} \end{aligned} \quad (56)$$

Substitution of (56) into (12) with $\eta = \pm 1$ leads to

$$-2cC_0 - dA_0 + \sum_{n=1}^{\infty} E_n \mathfrak{R}_n = 1 \quad (57)$$

where

$$\mathfrak{R}_n = \frac{2(-1)^n}{\zeta_n} \left[(1 - cp_1^2)(ep_2 - p_2^3) I_1(p_2 \zeta_n) \frac{I_1(p_1 \zeta_n)}{p_1} - (1 - cp_2^2)(ep_1 - p_1^3) I_1(p_1 \zeta_n) \frac{I_1(p_2 \zeta_n)}{p_2} \right] \quad (58)$$

In summary, for the unknown coefficients A_0, C_0, E_n and F_s , the coupled system of equations, (46), (47), (55) and (57), has to be solved simultaneously. In our numerical implementation, we can truncate the infinite series in these equations and retain only the first n and s terms. Then, there will be $(s+n+2)$ equations for the $(s+n+2)$ unknown

coefficients of A_0, C_0, E_n and F_s . Finally, A_n, B_n, C_s and D_s can be obtained by substitution of F_s and E_n into (34) and (35). Once these coefficients are determined, the stress and displacement fields inside the cylinder can be evaluated according to (24-27), and by substituting (24-25) into (1), the strain distribution can be exactly obtained.

9. Numerical results and discussions

The exact analytical solution for the inhomogeneous stress and strain distribution within a finite and transversely isotropic cylinder of wurtzite GaN under compression test with end friction given in the previous section involves the calculation of systems of coupled equations for the coefficients of the infinite series. We choose wurtzite GaN as an example to get the numerical results, and five independent elastic constants were $C_{11} = 293\text{GPa}$, $C_{12} = 159\text{GPa}$, $C_{13} = 106\text{GPa}$, $C_{33} = 398\text{GPa}$, $C_{44} = 105\text{GPa}$ (wright, 1997). Another group of independent constants can be easily obtained as $E_T = 322\text{GPa}$, $E_L = 357\text{GPa}$, $\nu_T = 0.32$, $\nu_L = 0.21$, $G_L = 52.5\text{GPa}$. In actual computation, the infinite series have to be truncated and only finite number of terms can be retained. It was found that 50 terms in both the summations of n and s are sufficient to yield a steady solution for the solutions for displacements expressed in (26-27), while about 80 terms are need to get a converge values for the series solutions for stresses and strain given in (24-25) and (1). This is not totally unexpected since our end boundary is displacement-controlled, and the computed stresses are proportional to the derivative of the displacement. In general, more terms in n than in s are needed if $\kappa > 1$, while more terms in s than in n are needed to get the same error control if $\kappa < 1$. We found that 100 terms in both s and n are enough to get a specific error control less than 0.1%. Moreover, the inhomogeneous strain and stress distributions within the finite circular cylinder for one quarter of the meridian plane are investigated, and the rest being symmetrical.

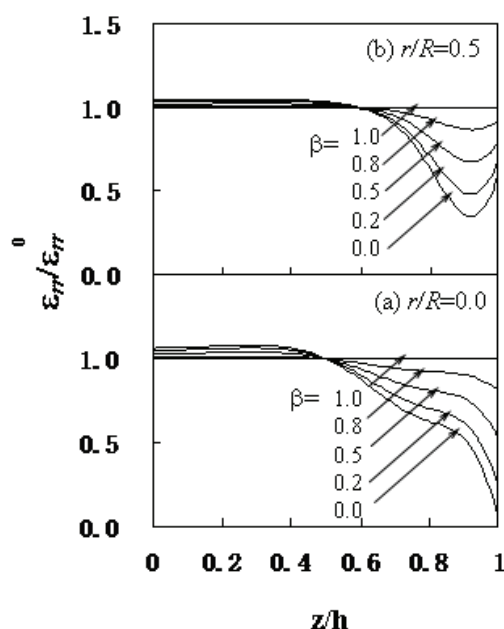


Fig. 2. The normalized strain $\varepsilon_{rr} / \varepsilon_{rr}^0$ versus the normalized distance z/h along the axis of loading for (a) $r/R=0.0$ and (b) $r/R=0.5$

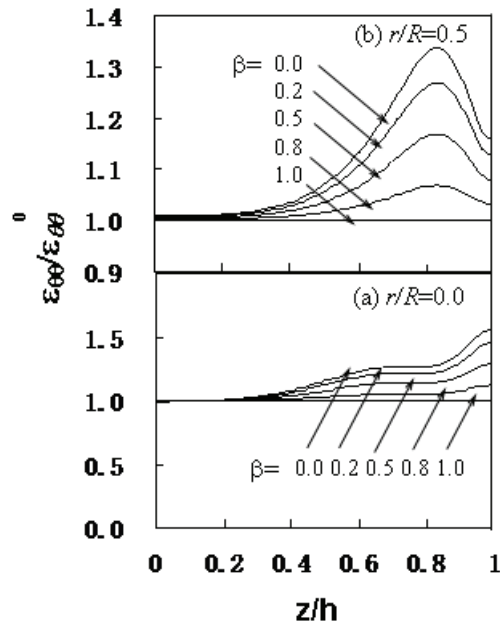


Fig. 3. The normalized strain $\varepsilon_{\theta\theta} / \varepsilon_{\theta\theta}^0$ versus the normalized distance z/h along the axis of loading for (a) $r/R=0.0$ and (b) $r/R=0.5$

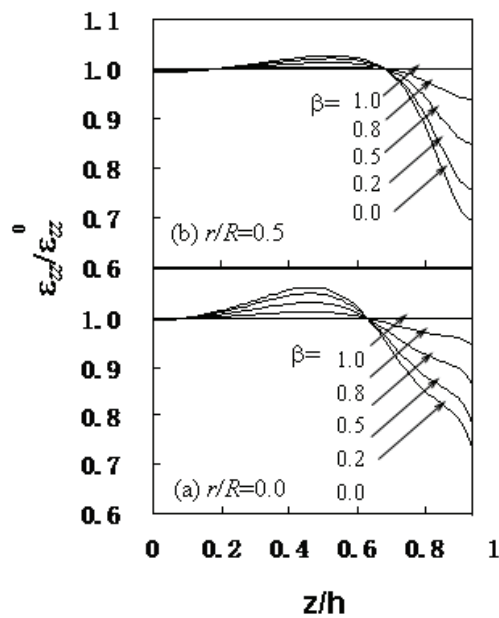


Fig. 4. The normalized strain $\varepsilon_{zz} / \varepsilon_{zz}^0$ versus the normalized distance z/h along the axis of loading for (a) $r/R=0.0$ and (b) $r/R=0.5$

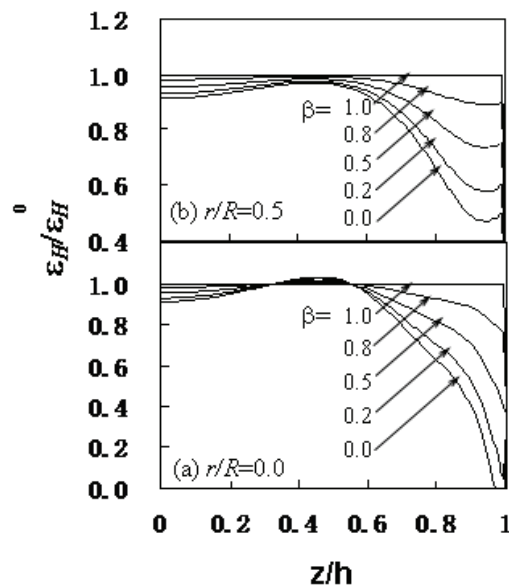


Fig. 5. The normalized strain $\varepsilon_H / \varepsilon_H^0$ versus the normalized distance z/h along the axis of loading for (a) $r/R=0.0$ and (b) $r/R=0.5$

9.1 The strain distributions within cylinder along the loading direction

Strain distributions along the loading direction in a quarter of the meridian plane are studied in this section. In particular, Fig. 2 shows the normalized strain $\varepsilon_{rr} / \varepsilon_{rr}^0$ versus the normalized vertical distance z/h from the center of the cylinder for various values of α for $r/R=0.0$ and $r/R=0.5$. The results are obtained for $h/R = 2.0$, which are the standard shape for compression tests. ε_{rr}^0 is the radial strain of the cylinder under compression without end friction and can be calculated according to (7). As mentioned earlier, the factor α represents the degree of friction on the end surfaces. More specially, $\beta = 1$ is for the case without end friction, while $\beta = 0$ is for the largest end friction and no slip occurs between the cylinder and the loading platens. In usual compression test, partial slip may occur and we have $0 \leq \beta \leq 1$, depending on the contact condition of the loading platens. Fig. 2 indicate that the strain distribution within the cylinder along the loading direction is not uniform for $0 \leq \beta < 1$, a strain concentrations are usually induced in the region of $0.5 < z/h < 1.0$, and the maximum values can be as more than 99% and 65% for $r/R=0.0$ and $r/R=0.5$ respectively, comparing to that without end friction, which is the line for $\alpha = 1$ in Fig. 2. However, the strain distributions in the central region, say $0 < z/h < 0.5$ are relatively uniform, and only 2% extra strain value of $\varepsilon_{rr} / \varepsilon_{rr}^0$ can be induced by end friction. Fig. 3 shows the normalized circumferential strain $\varepsilon_{\theta\theta} / \varepsilon_{\theta\theta}^0$ versus the normalized vertical distance z/h for various values of β for $r/R=0.0$ and $r/R=0.5$, and $\varepsilon_{\theta\theta}^0$ is the circumferential strain of the cylinder under compression without end friction and can be calculated according to (7). The other parameters used in Fig. 3 and the following Figs. 4-12 are the same as those in Fig. 2 unless specially mentioned. Fig.3 shows that strain concentrations are also induced in the region of $0.5 < z/h < 1.0$, and the maximum values can be as more than 57% and 34% for $r/R=0.0$ and $r/R=0.5$ respectively, comparing

to constant strain without end friction and $\alpha = 1$. Fig. 4 shows the normalized axial strain $\varepsilon_{zz} / \varepsilon_{zz}^0$ versus the normalized vertical distance z/h for various values of α for $r/R=0.0$ and $r/R=0.5$, and ε_{zz}^0 is the axial strain of the cylinder under compression without end friction and can be calculated according to (7). Fig.4 shows that the axial strain is also inhomogeneous, and the maximum values can be more than 40% and 30% for $r/R=0.0$ and $r/R=0.5$ respectively, comparing to that without end friction. Fig. 5 shows the normalized strain $\varepsilon_H / \varepsilon_H^0$ versus the normalized vertical distance z/h for various values of α for $r/R=0.0$ and $r/R=0.5$, and ε_H^0 is the strain of the cylinder under compression without end friction and can be calculated according to (58). Fig.5 shows that the normalized strain $\varepsilon_H / \varepsilon_H^0$ is quite inhomogeneous, and the maximum values can be 100% and 53% more than those without end friction for $r/R=0.0$ and $r/R=0.5$ respectively. Overall, the inhomogeneous strain distributions are induced in the cylinder as long as friction exists between the end surface and the loading platens, and the larger the friction on the end surfaces, that is, the smaller the value of β , the more non-uniform inhomogeneous strain is induced within the cylinder.

9.2 The strain distributions within cylinder for different shape of cylinder

All of the numerical calculations given above are for $h / R = 2.0$. In order to investigate the shape effect on the strain distribution within cylinder under compression with end friction, Figs. 6-8 plot the normalized strains $\varepsilon_{rr} / \varepsilon_{rr}^0$, $\varepsilon_{\theta\theta} / \varepsilon_{\theta\theta}^0$ and $\varepsilon_{zz} / \varepsilon_{zz}^0$ versus the normalized vertical distance z/h from the center of the cylinder for various values of h/R for $r/R=0.0$ and $\beta=0.0$. Figs. 6-8 show that a larger deviation may be induced for shorter cylinder. For example, 35% error in $\varepsilon_H / \varepsilon_H^0$ can be induced even at the center of the cylinder for $h/R=0.5$. But the strain distributions for long cylinders are more homogeneous, especially the strains are relatively uniform at the central part of the cylinder if $h / R \geq 2$. So a relatively long cylinder should be suggested for compression test.

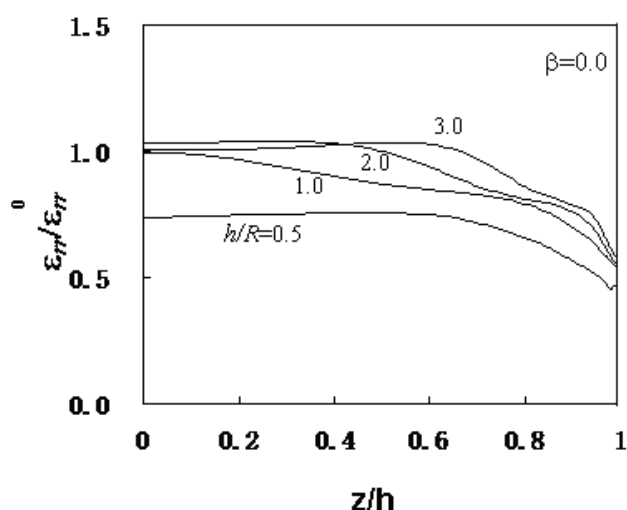


Fig. 6. The normalized strain $\varepsilon_{rr} / \varepsilon_{rr}^0$ versus the normalized distance z/h along the axis of loading for various ratios of h/R

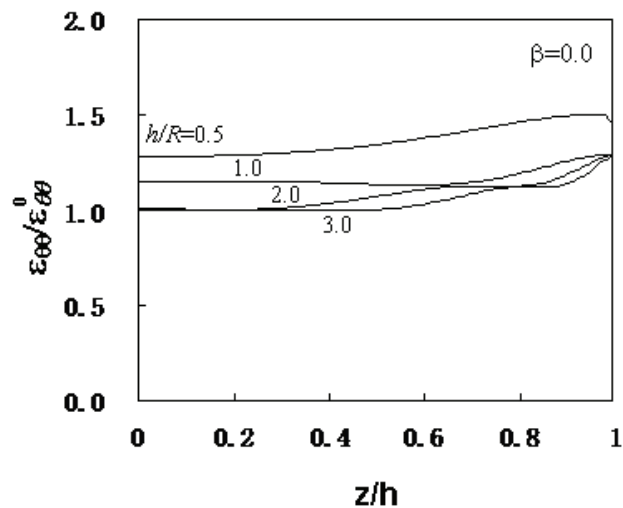


Fig. 7. The normalized strain $\varepsilon_{\theta\theta} / \varepsilon_{\theta\theta}^0$ versus the normalized distance z/h along the axis of loading for various ratios of h/R

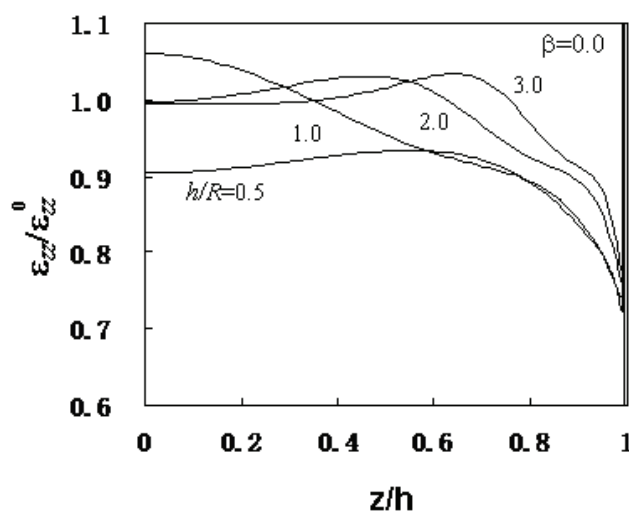


Fig. 8. The normalized strain $\varepsilon_{zz} / \varepsilon_{zz}^0$ versus the normalized distance z/h along the axis of loading for various ratios of h/R

10. The effect of strain on the valence-band structure of wurtzite GaN

The band structure of wurtzite GaN deserves attention since the valence bands, such as the heavy-hole, light-hole and split-off bands are close each other. The strain effects on wurtzite GaN are less understood (Chuang & Chang, 1996). Based on the deformation potential theory of Luttinger-Kohn and Bir-Pikus (Bir & Pickus, 1974), the valence-band structure of the strained wurtzite GaN can be described by a 6x6 Hamiltonian according to the envelope-function method, and the basis function for wurtzite GaN can be written as

$$\begin{aligned}
 |1\rangle &= -\frac{\alpha^*}{\sqrt{2}}|(X+iY)\uparrow\rangle + \frac{\alpha}{\sqrt{2}}|(X-iY)\downarrow\rangle \\
 |2\rangle &= -\frac{\beta}{\sqrt{2}}|(X-iY)\uparrow\rangle - \frac{\beta^*}{\sqrt{2}}|(X+iY)\downarrow\rangle \\
 |3\rangle &= \beta^*|Z\uparrow\rangle + \beta|Z\downarrow\rangle \\
 |4\rangle &= -\frac{\alpha^*}{\sqrt{2}}|(X+iY)\uparrow\rangle - \frac{\alpha}{\sqrt{2}}|(X-iY)\downarrow\rangle \\
 |5\rangle &= \frac{\beta}{\sqrt{2}}|(X-iY)\uparrow\rangle + \frac{\beta^*}{\sqrt{2}}|(X+iY)\downarrow\rangle \\
 |6\rangle &= -\beta^*|Z\uparrow\rangle + \beta|Z\downarrow\rangle
 \end{aligned}
 \tag{59}$$

where $\alpha = (1/\sqrt{2})e^{i(3\pi/4+3\phi/2)}$, $\beta = (1/\sqrt{2})e^{i(\pi/4+\phi/2)}$ and $\phi = \tan^{-1}(k_y/k_x)$.

The 6x6 Hamiltonian is obtained as

$$H(k) = \begin{bmatrix} H_{3\times 3}^U(k) & 0 \\ 0 & H_{3\times 3}^L(k) \end{bmatrix}
 \tag{60}$$

and

$$H_{3\times 3}^U = \begin{bmatrix} F_t & K_t & -iH_t \\ K_t & G_t & \Delta - iH_t \\ iH_t & \Delta + iH_t & \lambda_t \end{bmatrix}
 \tag{61}$$

$$H_{3\times 3}^L = \begin{bmatrix} F_t & K_t & iH_t \\ K_t & G_t & \Delta + iH_t \\ -iH_t & \Delta - iH_t & \lambda_t \end{bmatrix}
 \tag{62}$$

$$F_t = \Delta_1 + \Delta_2 + \lambda_t + \theta_t
 \tag{63}$$

$$G_t = \Delta_1 - \Delta_2 + \lambda_t + \theta_t
 \tag{64}$$

$$\lambda_t = \frac{\hbar^2}{2m_0} [A_{t1}k_z^2 + A_{t2}(k_x^2 + k_y^2)] + D_1\varepsilon_{zz} + D_2(\varepsilon_{xx} + \varepsilon_{yy})
 \tag{65}$$

$$\theta_t = \frac{\hbar^2}{2m_0} [A_{t3}k_z^2 + A_{t4}(k_x^2 + k_y^2)] + D_3\varepsilon_{zz} + D_4(\varepsilon_{xx} + \varepsilon_{yy})
 \tag{66}$$

$$K_t = \frac{\hbar^2}{2m_0} A_{t5}(k_x^2 + k_y^2)
 \tag{67}$$

$$H_t = \frac{\hbar^2}{2m_0} A_{t6} (k_x^2 + k_y^2)^{1/2} k_z \quad (68)$$

$$\Delta = \sqrt{2} \Delta_3 \quad (69)$$

where

$$A_{t3} = -2A_{t4} = A_{t2} - A_{t1} \quad (70)$$

$$A_{t3} + 4A_{t5} = \sqrt{2} A_{t6} \quad (71)$$

$$\Delta_3 = \Delta_2 \quad (72)$$

The valence-band structure can be determined by

$$\det[H(k) - EI] = 0 \quad (73)$$

which leads to

$$(E^3 + C_{t2}E^2 + C_{t1}E + C_{t0})^2 = 0 \quad (74)$$

where

$$C_{t2} = -(F_t + G_t + \lambda_t) \quad (75)$$

$$C_{t1} = F_t G_t + G_t \lambda_t + F_t \lambda_t - \Delta^2 - K_t^2 - 2H_t^2 \quad (76)$$

$$C_0 = -\det[H_{3 \times 3}^U] \quad (77)$$

so we obtained

$$E_{HH} = F_t \quad (78)$$

$$E_{LH} = \frac{G_t + \lambda_t}{2} + \sqrt{\frac{(G_t - \lambda_t)^2}{2} + \Delta^2} \quad (79)$$

$$E_{SO} = \frac{G_t + \lambda_t}{2} - \sqrt{\frac{(G_t - \lambda_t)^2}{2} + \Delta^2} \quad (80)$$

where E_{HH} , E_{LH} and E_{SO} are the energies for the heavy-hole the light-hole and split-off bands, respectively.

11. Conclusions

The exact analytical solution for the inhomogeneous strain field within a finite and transversely isotropic cylinder under compression test with end friction is derived. The method employed Lekhnitskii's stress function in order to uncouple the equations of

equilibrium. It was found that the end friction leads to a very inhomogeneous strain distribution within cylinder, especially in the area near the end surface. Numerical results show that all of the strain components, including the axial, radial, circumferential and shear strains, are inhomogeneous, both in distribution pattern and magnitude, the maximum value of the strain concentration near the end surfaces can be 100% higher than the constant strain in the case without end friction. However, the strain distributions are relatively uniform at the central parts of long cylinders, say in the area of $-0.5h < z < 0.5h$, the magnitude of the strains can be more than 2% of that without end friction. The method for analyzing the effect of the strain and end friction on the band structure of wurtzite GaN is discussed, end friction has effect on the shape of constant energy surfaces of valence bands and the band gaps between the heavy-hole, light-hole and split-off bands of wurtzite GaN.

12. Acknowledgment

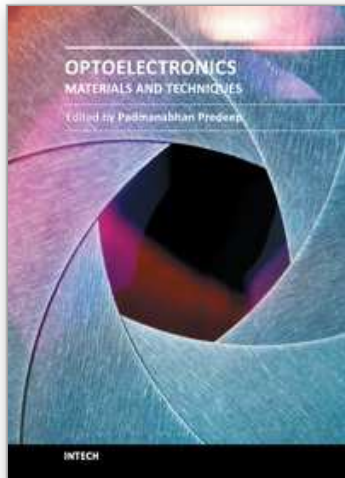
This work was supported by the National Natural Science Foundation of China (Grant No. 11032003 and 10872033) and the State Key Laboratory of Explosion Science and Technology.

13. References

- Bir, G. L. & Pickus, G. E. (1974). *Symmetry and Strain Induced Effects in Semiconductors*, John Wiley, New York, USA
- Chau K. T. & Wei, X. X(1999). Finite solid circular cylinders subjected to arbitrary surface load: part I. Analytic solution. *International Journal of Solids and Structures*, Vol. 37, pp. 5707-5732
- Choi, S. W. & Shah, S. P. (1998). Fracture mechanism in cement-based materials subjected to compression. *Journal of Engineering Mechanics ASCE*, Vol. 124, pp. 94-102
- Chuang, S. L. & Chang, C. S. (1996), k-p method for strained wurtzite semiconductors. *Physical Review B*, Vol. 54, pp. 2491-2504
- Goroff, I. & Kleinman, L. (1963). Deformation potentials in silicon. III. effects of a general strain on conduction and valence levels. *Physical Review*, Vol. 132, pp. 1080-1084
- Hasegawa, H. (1963). Theory of cyclotron resonance in strained silicon crystals. *Physical Review*, Vol. 129, pp. 1029-1040
- Hussein, A & Marzouk, H(2000). Finite element evaluation of the boundary conditions for biaxial testing of high strength concrete. *Material Structure*, Vol. 33, pp. 299-308
- Jiang, H. & Singh, J. (1997). Strain distribution and electronic spectra of InAs/GaAs self-assembled dots: An eight-band study. *Physical Review B*, Vol. 56, pp. 4696-4701
- Lekhnitskii, S. G(1963). *Theory of elasticity of an anisotropic elastic body*, English translation by P. Fern, Holden-Day Inc., San Francisco, USA
- Mathieu, H. ; Mele, P. and Ameziane, E. L., et al (1979). Deformation potentials of the direct and indirect absorption edges of GaP. *Physical Review B*, Vol. 19, pp. 2209-2223
- Pollak, F. H. & Cardona, M. (1968). Piezo-Electroreflectance in Ge, GaAs, and Si. *Physical Review*, Vol. 172, pp 816-837
- Pollak, F. H. (1990). *In Strained-Layer Superlattices*, edited by T. Pearsall, Semiconductors and Semimetals, Academic, Boston, , USA
- Suzuki, K. & Hensel, J. C. (1974). Quantum resonances in the valence bands of germanium. I. Theoretical considerations. *Physical Review B*, Vool. 9, pp 4184-4218

- Singh, J. (1992). *Physics of Semiconductors and Their Heterostructures*, McGraw-Hill Higher Education, New York, USA
- Torrenti, J.M. ; Benaija, E. H. & Boulay, C. (1993). Influence of boundary conditions on strain softening in concrete compression test. *Journal of Engineering Mechanics ASCE*, Vol. 119, pp. 2369-2384
- Wei, X. X. ; Chau, K. T. & Wong, R. H. C. (1999). A new analytic solution for the axial point load strength test for solid circular cylinders. *Journal of Engineering Mechanics*, Vol. 125, pp. 1349-1357
- Wei, X. X. (2008). Non-uniform strain field in a wurtzite GaN cylinder under compression and the related end friction effect on quantum behavior of valence-bands. *Mechanics of Advanced Materials and Structures*, Vol. 15, pp. 612-622
- Wright, A. F. (1997). Elastic properties of zinc-blende and wurtzite AlN, GaN, and InN. *Journal of Applied Physics*, Vol. 82, pp. 2833-2839

IntechOpen



Optoelectronics - Materials and Techniques

Edited by Prof. P. Predeep

ISBN 978-953-307-276-0

Hard cover, 484 pages

Publisher InTech

Published online 26, September, 2011

Published in print edition September, 2011

Optoelectronics - Materials and Techniques is the first part of an edited anthology on the multifaceted areas of optoelectronics by a selected group of authors including promising novices to the experts in the field. Photonics and optoelectronics are making an impact multiple times the semiconductor revolution made on the quality of our life. In telecommunication, entertainment devices, computational techniques, clean energy harvesting, medical instrumentation, materials and device characterization and scores of other areas of R&D the science of optics and electronics get coupled by fine technology advances to make incredibly large strides. The technology of light has advanced to a stage where disciplines sans boundaries are finding it indispensable. Smart materials and devices are fast emerging and being tested and applications developed in an unimaginable pace and speed. Here has been made an attempt to capture some of the materials and techniques and underlying physical and technical phenomena that make such developments possible through some real time players in the field contributing their work and this is sure to make this collection of essays extremely useful to students and other stake holders such as researchers and materials scientists in the area of optoelectronics.

How to reference

In order to correctly reference this scholarly work, feel free to copy and paste the following:

X. X. Wei (2011). An Analytical Solution for Inhomogeneous Strain Fields Within Wurtzite GaN Cylinders Under Compression Test, Optoelectronics - Materials and Techniques, Prof. P. Predeep (Ed.), ISBN: 978-953-307-276-0, InTech, Available from: <http://www.intechopen.com/books/optoelectronics-materials-and-techniques/an-analytical-solution-for-inhomogeneous-strain-fields-within-wurtzite-gan-cylinders-under-compressi>

INTECH
open science | open minds

InTech Europe

University Campus STeP Ri
Slavka Krautzeka 83/A
51000 Rijeka, Croatia
Phone: +385 (51) 770 447
Fax: +385 (51) 686 166
www.intechopen.com

InTech China

Unit 405, Office Block, Hotel Equatorial Shanghai
No.65, Yan An Road (West), Shanghai, 200040, China
中国上海市延安西路65号上海国际贵都大饭店办公楼405单元
Phone: +86-21-62489820
Fax: +86-21-62489821

© 2011 The Author(s). Licensee IntechOpen. This chapter is distributed under the terms of the [Creative Commons Attribution-NonCommercial-ShareAlike-3.0 License](#), which permits use, distribution and reproduction for non-commercial purposes, provided the original is properly cited and derivative works building on this content are distributed under the same license.

IntechOpen

IntechOpen